
VISUALIZING THE FINER CLUSTER STRUCTURE OF LARGE-SCALE AND HIGH-DIMENSIONAL DATA

Yu Liang*, Arin Chaudhuri, and Haoyu Wang

IoT Analytics, SAS Inc.
701 SAS Campus Drive, Cary, NC 27519
*Corresponding author: Yu Liang, yu.liang@sas.com

July 20, 2020

ABSTRACT

Dimension reduction and visualization of high-dimensional data have become very important research topics because of the rapid growth of large databases in data science. In this paper, we propose using a generalized sigmoid function to model the distance similarity in both high- and low-dimensional spaces. In particular, the parameter b is introduced to the generalized sigmoid function in low-dimensional space, so that we can adjust the heaviness of the function tail by changing the value of b . Using both simulated and real-world data sets, we show that our proposed method can generate visualization results comparable to those of uniform manifold approximation and projection (UMAP), which is a newly developed manifold learning technique with fast running speed, better global structure, and scalability to massive data sets. In addition, according to the purpose of the study and the data structure, we can decrease or increase the value of b to either reveal the finer cluster structure of the data or maintain the neighborhood continuity of the embedding for better visualization. Finally, we use domain knowledge to demonstrate that the finer subclusters revealed with small values of b are meaningful.

Keywords Dimension Reduction · Manifold Learning · Data Visualization

1 Introduction

Dimension reduction and visualization of high-dimensional data have become very important research topics in many scientific fields because of the rapid growth of data sets with large sample size and/or dimensions.

In the literature of dimension reduction and information visualization, linear methods such as principal component analysis (PCA) [7] and classical scaling [17] mainly focus on preserving the most significant structure or maximum variance in data; nonlinear methods such as multidimensional scaling [2], isomap [16], and curvilinear component analysis (CCA) [5] mainly focus on preserving the long or short distances in the high-dimensional space. They generally perform well in preserving the global structure of data but can fail to preserve the local structure. In recent years, the manifold learning methods, such as SNE [6], Laplacian eigenmap [1], LINE [15], LARGEVIS [14], t-SNE [19] [18], and UMAP [10], have gained popularity because of their ability to preserve both the local and some aspects of the global structure of data. These methods generally assume that data lie on a low-dimensional manifold of the high-dimensional input space. They seek to find the manifold that preserves the intrinsic structure of the high-dimensional data.

Many of the manifold learning methods suffer from something called the “crowding problem” while preserving local distance of high-dimensional data in low-dimensional space. This means that, if you want to describe small distances in high-dimensional space faithfully, the points with moderate or large distances between them in high-dimensional space are placed too far away from each other in low-dimensional space. Therefore, in the visualization, the points with small or moderate distances between them crash together. To solve this problem, UNI-SNE [4] adds a slight repulsion strength to any pair of points in low-dimensional space to prevent the points from moving too far away from each

other. Alternatively, t-SNE [19] [18] uses the Student’s t -distribution in low-dimensional space, which has a heavy tail compared with the Gaussian distribution used in high-dimensional space. Kobak et al. [8] further extended the idea to use the t -distribution with one degree of freedom v . They show that for some data sets, setting $v < 1$ would reveal additional local structure of the data compared with the Student’s t -distribution with $v = 1$. On the other hand, UMAP uses a curve that is similar to the t -distribution but with two hyperparameters, a^* and b^* , in low-dimensional space. The two parameters are estimated by approximating an exponential function with the parameter min_dist . By adjusting min_dist , UMAP governs the appearance of the embedding.

In this paper, we propose using a generalized sigmoid function to model the distance similarity in both high- and low-dimensional spaces. In particular, the parameter b is introduced to the generalized sigmoid function in low-dimensional space, and we can adjust the heaviness of the function tail by changing the value of b . We use both simulated and real-world data sets to show that our proposed method can generate visualization results that are competitive with those of UMAP. In addition, b can be easily adjusted either to reveal the finer cluster structure of the data or to assist the visualization of data by increasing the continuity of neighbors. For some data sets, decreasing the value of b can provide greater visibility of the intrinsic structure of the data that might not be visible using conventional UMAP. Finally, we use domain knowledge to demonstrate that the finer subclusters are meaningful.

2 Methodology

Let $X = \{x_1, \dots, x_N\}$ be N input data in high-dimensional space R^D , and let $d(x_i, x_j)$ be the distance between x_i and x_j under the metric $d : X \times X \rightarrow \mathbb{R}_{\geq 0}$. Let $N(x_i)$ be the k -nearest neighbors of x_i , and let ρ_i be the shortest distance from x_i to its k -nearest neighbors. Here ρ_i is defined as

$$\rho_i = \min\{d(x_i, x_j) | d(x_i, x_j) > 0, x_j \in N(x_i), 1 \leq j \leq k\}, \quad 1 \leq i \leq N$$

For each x_i , we use the sigmoid function with the parameter σ_i to model the distance similarity between points x_i and x_j , which is

$$P_{j|i} = \begin{cases} \frac{1.0}{1.0 + \frac{\max(0, d(x_i, x_j) - \rho_i)}{\sigma_i}} & \text{if } x_j \in N(x_i) \\ 0 & \text{otherwise} \end{cases}$$

Using the same approach as UMAP, we can determine the value of σ_i through the following equation:

$$\sum_{j=1}^k P_{j|i} = \log_2(k)$$

For the simplicity of optimizing the loss function and also extracting more structure information in high-dimensional space, $P(j|i)$ is symmetrized as

$$P_{ij} = P_{j|i} + P_{i|j} - P_{i|j} \odot P_{j|i}$$

where \odot stands for componentwise multiplication. In addition, let $P_{N \times N}$ denote the matrix of P_{ij} .

Let $Y = \{y_1, \dots, y_N\}$ denote the representation of X in low-dimensional space. UMAP uses the curve

$$Q(i, j) = \frac{1}{(1 + a^* \|y_i - y_j\|_2^{2b^*})}$$

to model the distance distribution in low-dimensional space, where $\|y_i - y_j\|_2$ stands for the distance between points y_i and y_j . The curve is similar to the t distribution with two parameters, a^* and b^* , which are estimated by approximating the following function:

$$\Phi(y_i, y_j) = \begin{cases} 1 & \text{if } \|y_i - y_j\|_2 \leq min_dist \\ \exp(-(\|y_i - y_j\|_2 - min_dist)) & \text{otherwise} \end{cases}$$

The parameter min_dist is an important parameter in the UMAP algorithm. It controls how closely the points in low-dimensional representations are packed together. The larger the value of min_dist is, the more the embeddings spread out; the smaller the value of min_dist is, the more likely the data in the same cluster are densely packed. As shown in our experiments, when the value of min_dist is smaller than 0.01, further decreasing the value of min_dist usually does not change the embeddings much. In order to reveal a finer cluster structure, manually decreasing the values of parameters a^* and b^* might be needed. However, because there are two hyperparameters, more experiments might be necessary to find the proper values of a^* and b^* . This is beyond the scope of the paper.

Here we assume that the membership strength of y_i and y_j can be modeled using a generalized sigmoid function [3], which can be expressed as

$$Q(i, j) = \frac{1.0}{\left[1.0 + (2^{u/v} - 1) \left(\frac{\|y_i - y_j\|_2}{s}\right)^u\right]^{v/u}} \quad (1)$$

Let $a = u$ and $b = v/u$. Then Equation (1) can be rewritten as

$$Q(i, j) = \frac{1.0}{\left[1.0 + (2^{1/b} - 1) \left(\frac{\|y_i - y_j\|_2}{s}\right)^a\right]^b} \quad (2)$$

When $b = 1$, $Q(i, j)$ becomes

$$Q(i, j) = \frac{1.0}{\left[1.0 + \left(\frac{\|y_i - y_j\|_2}{s}\right)^a\right]}$$

This is equivalent to the model of UMAP with $a = 2b^*$ and $s^{-a} = a^*$.

Here we consider a simplified version of $Q(i, j)$ by rescaling $\|y_i - y_j\|_2$ by s , so that we have

$$Q(i, j) = \frac{1.0}{\left[1.0 + (2^{1/b} - 1)\|y_i - y_j\|_2^a\right]^b} \quad (3)$$

In other words, the solution of Equation (3) will have a scale change by s compared with the solution of Equation (2).

As with the probabilistic model [14], the loss function can be written as

$$L = - \left(\sum_{(x_i, x_j) \in E} P_{ij} \log Q(i, j) + \sum_{(x_i, x_j) \notin E} \log(1 - Q(i, j)) \right)$$

where E is the collection of points (x_i, x_j) for which either $x_i \in N(x_j)$ or $x_j \in N(x_i)$.

Using the negative sampling strategy proposed by [11], the loss function can be further written as

$$L = - \left(\sum_{(x_i, x_j) \in E} P_{ij} \log Q(i, j) + \sum_{k=1}^M \log(1 - Q(i, k)) \right)$$

where M is the number of negative samples for each vertex i . The gradient of the loss function can be written as

$$\frac{\partial L}{\partial y_i} = - \left(\sum_{(i, j) \in E} P_{ij} \frac{\partial Q(i, j) / \partial y_i}{Q(i, j)} - \sum_{k=1}^M \frac{\partial Q(i, k) / \partial y_i}{(1 - Q(i, k))} \right)$$

where

$$\partial Q(i, j) / \partial y_i = -ab \left(1.0 + (2^{1/b} - 1)\|y_i - y_j\|_2^a\right)^{-b-1} (2^{1/b} - 1)\|y_i - y_j\|_2^{a-2} (y_i - y_j)$$

As with UMAP, the stochastic gradient descent algorithm can be used to optimize the loss function.

In our experiments, we found that the proper range of a is $[1, 1.5]$. The value of a is less important than the value of b , and setting $a = 1$ generally gives us satisfactory results. So, in our experiments, we set $a = 1$. Because b controls the rate of the curve approaching 0 and 1, adjusting the value of b can affect the embeddings in low-dimensional space and the data visualization. To understand how the family of Equation (3) behaves with varying b , we draw plots by setting $a = 1$ and $b = 0.5, 1, 2, 5, 10$. The results are summarized in Figure 1.

We can see from the graph that the smaller the b value is, the more heavy-tailed the curve is. The heavy-tail property of the curve can greatly alleviate the crowding problem when you are embedding high-dimensional data in low-dimensional space and thus provide the possibility of revealing the finer structure of the data.

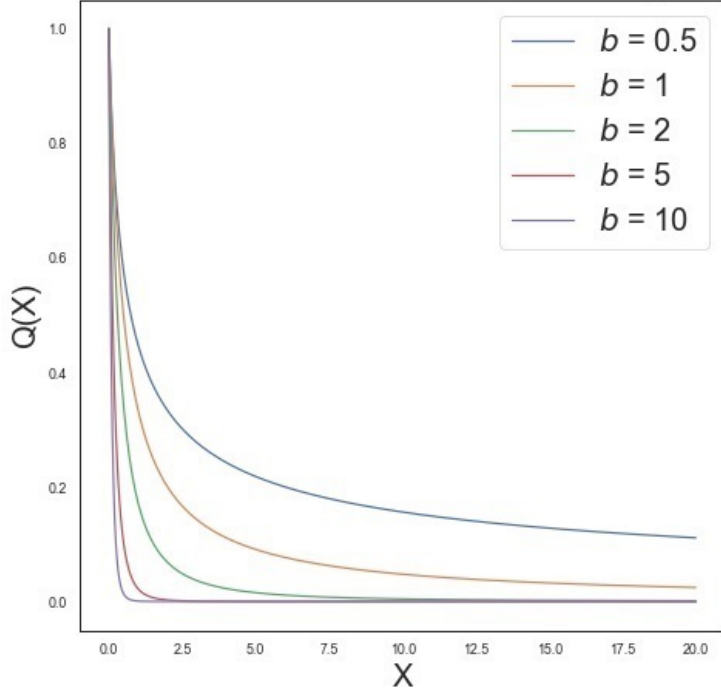


Figure 1: The distance similarity in low-dimensional space is modeled by the function in Equation (3). The graph shows the curve changes with $a = 1$ and $b = 0.5, 1, 2, 5,$ and 10 .

3 Experimental Results

3.1 Simulated Data

To study the embeddings with different b values, we randomly generate a data set that contains 1,000 data points and 20 dimensions. These data points are evenly distributed among 10 clusters (each cluster has 100 data points). Within each cluster, the first 50 data points are randomly sampled from a Gaussian distribution with mean $\mu_i = 5e_i + 2.3e_{10+i}$; and the other 50 data points have mean $\mu_i = 5e_i - 2.3e_{10+i}$, where e_i is the i th basis vector and $i = 1, 2, \dots, 10$. All the data points have covariance I_{20} . The similar experiment is also considered in [8]. In this experiment, we set $k = 10$ (10 nearest neighbors), $a = 1$, and $b = 0.5, 1, 2,$ and 10 . For comparison, we also run UMAP by setting $k = 10$, and $min_dist = 0.001, 0.01, 0.1,$ and 1 . For both settings, the initial values of the embedding are set to be the eigenvectors of the normalized Laplacian. And 500 epochs are used in the stochastic gradient descent algorithm. The results are summarized in Figure 2.

From the setup, we expect that the data will be separated into 10 distinct clusters. Within each big cluster, the data can be classified into two subclusters or at least have a “dumbbell” shape, because they have different mean values.

We can see from the embeddings, for our proposed method, that all the big clusters are well separated from each other with various values of b . In addition, when $b = 0.5$ or $b = 1$, the majority of the big clusters are separated into two isolated subclusters. For the rest of the big clusters, we can see the dumbbell shape very well. With the value b increasing, the two subclusters within each cluster get closer and closer and eventually merge into one cluster. However, even with $b = 10$, we can still see the dumbbell shape within each big cluster.

For UMAP, even with $min_dist = 0.001$, the subclusters within each big cluster are not well separated. However, we can still see the dumbbell shape for some of the clusters, such as the blue, light red, and yellow clusters. With the increases of min_dist , the distances between different clusters decrease. In addition, we further lose the dumbbell shapes within several clusters. We also notice that there is not much difference between the graphs with $min_dist = 0.001$ and the graphs with $min_dist = 0.01$. A possible reason is that when $min_dist \leq 0.01$, further decreasing the value of min_dist does not change the values of a^* and b^* much.

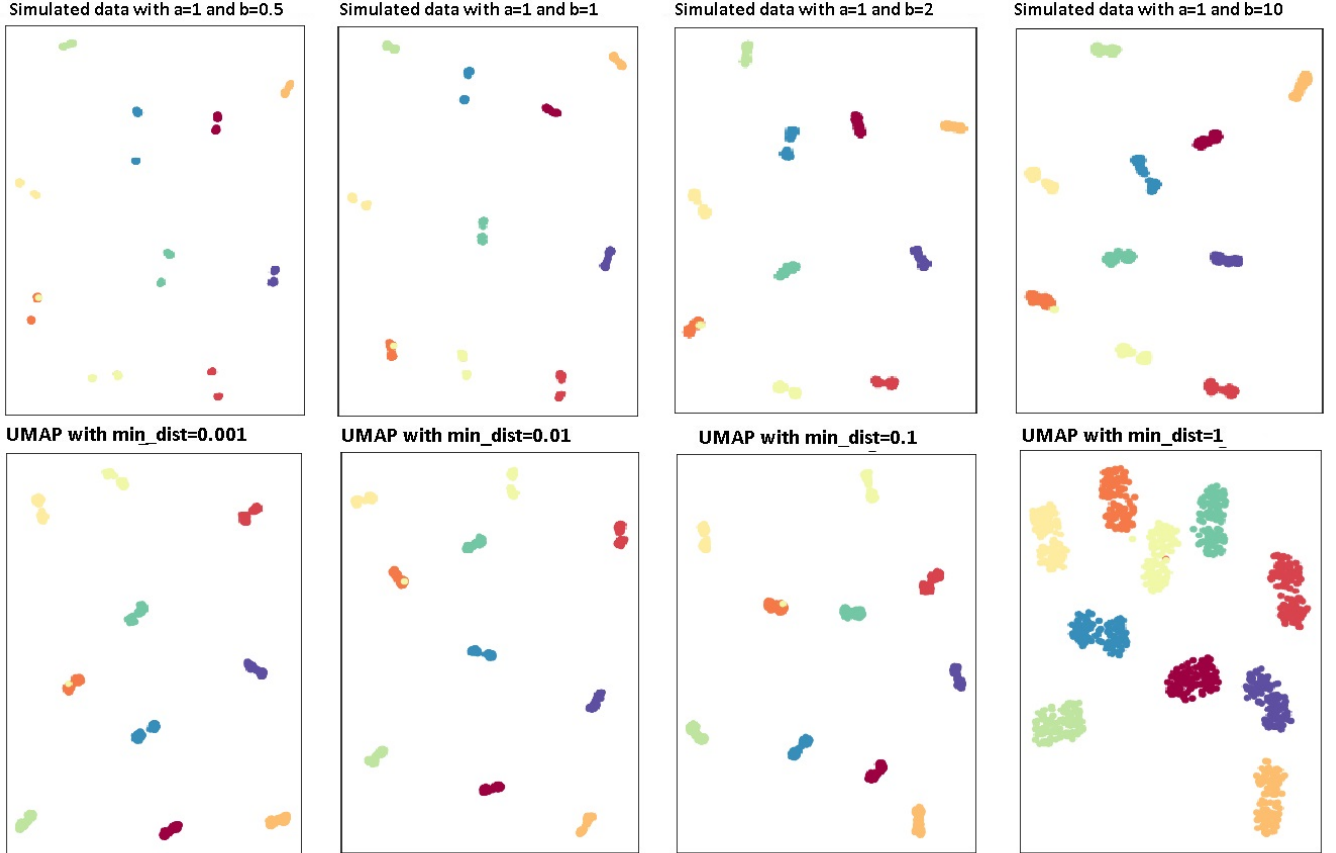


Figure 2: Embeddings comparison using simulated data. For our proposed method, the graphs are generated by setting $b = 0.5, 1, 2,$ and $10,$ respectively. For UMAP, the graphs are generated by setting $min_dist = 0.001, 0.01, 0.1,$ and $1,$ respectively.

3.2 Real Data Sets

To further test the performance of our proposed method, we apply the method to the following real data sets with either large or small sample sizes:

1. MNIST [9]: Data set includes 70,000 images of the handwritten digits 0–9. Each image is 28×28 pixels in size.
2. Fashion-MNIST [20]: Data set includes 70,000 images of 10 classes of fashion items (clothing, footwear, and bags). Because the images are gray-scale images, 28×28 pixels in size, the feature dimension is 784.
3. Turbofan Engine Degradation Simulation data set [13]: Engine degradation data are simulated under different combinations of operational conditions. In the data set, 21 sensor measurements for 260 engines under six operational conditions are recorded until the engine fails. We assume that all the engines operate normally at the beginning of the study. There are a total 53,759 observations in the data set.

4. COIL-20 [12]: Data set includes 1,440 gray-scale images, 28×28 pixels in size, of 20 objects under 72 rotations spanning 360 degrees.

For all the data sets, we considered Euclidean distance. We set $k = 10$ and vary b values from 1, 2, 5, to 10. As with the simulated data, the initial values of the embedding are set to be the eigenvectors of the normalized Laplacian. The visualizations are summarized in Figure 3.

We can see from the graphs, that when $b = 1$, the clusters for each data set have the biggest separation and the greatest distance. For example, all the digits are separated into distinct clusters in the MNIST data set when $b = 1$. With the increases in the value of b , the distances between different digits get smaller and smaller. Some digits, such as 4, 7, and 9, and 3, 5, and 8, join together eventually. Based on the embeddings, we use k -means to do classification and find that when $b = 1$ and $b = 2$, we get the smallest error, 4.4%.

For the Fashion-MNIST data set, with various b values, trousers (red) and bags (blue) always have the greatest distance from each other. In addition, shoes, bags, trousers, and other clothes (T-shirts, dresses, pullovers, shirts, and coats) are well separated when $b = 1$ or $b = 2$. When $b = 5$ and $b = 10$, bags, and other clothes get much closer to each other. They are not distinct clusters anymore. It is also worth pointing out that when $b = 1$ or $b = 2$, we also see a few subclusters that are invisible when $b = 5$ or $b = 10$. For example, the majority of the T-shirts (dark red) and dresses (orange) are separated from coats (yellow), pullovers (vermilion), and shirts (light green); sneakers (green), ankle boots (purple), and sandals (lemon) have certain separation as well. In addition, sandals are now separated into two subclusters. Among them, one subcluster is close to sneakers and the other is close to ankle boots. Furthermore, bags (blue) are separated into two subclusters as well.

To verify whether these subclusters are meaningful or not, we randomly sampled 100 images from each of the subclusters that we mentioned earlier and compared the images. We found that the separation of T-shirts and dresses from other clothing is due to long or short sleeves. For bags, in one subcluster, the majority of the bags have handles showing at the top of the image. However, in the other subcluster, either the bags do not have a handle or the handle is not showing at the top of the image. In addition, the images of sandals also show that the majority of the sandals in one subcluster have middle or high heels, whereas the sandals in the other subcluster are relatively flat. These image comparisons clearly show that the subclusters revealed by small b values are meaningful. They provide additional insights into the data structure of Fashion-MNIST. The comparison results are summarized in Figure 4.

In the Turbofan Engine Degradation Simulation data set, the flight condition indicator is removed from the data. Using the readings only from 21 sensors, our proposed method successfully classified the data into six categories with high accuracy. For each cluster, we can see that the readings that are taken close to the fault points are approximately on the edge of the embedding (blue color). To further investigate the engine degradation process, we remove the impact of different flight conditions by subtracting the average reading measurement for each sensor at each flight condition and redo the embedding. The resulting embeddings are shown in Figure 5.

The embeddings clearly show that the sensor readings in the early stage of the study mainly concentrate on one side of the graph and the readings close to the fault points mainly concentrate on the other side of the graph with the tail. With a small value of b , we can see that the readings recorded at a similar stage of an engine’s life cycle tend to concentrate together.

For the COIL-20 data set, with different b values, the majority of the objects are well separated, except for cars (objects 3, 6, and 19), Anacin, and Tylenol. With the increases in the value of b , the between-class distance for different objects gets smaller and smaller, which can cause problems for data clustering. However, we can see more clearly the circular structure of each object with a higher value of b . One interesting fact is that we find that object 1 is classified into three subclusters (light blue color). We randomly sampled some of the images from each subcluster and found that the subclusters are formed mainly according to the direction of the arrow (downward, upward, and horizontally). Some of the images are displayed in Figure 6.

For comparison, we also run UMAP by setting $k = 10$ and min_dist to 0.001, 0.01, 0.1, and 1 while keeping other settings the same as in our proposed method. The results are summarized in Figure 7. From the graph we can see that UMAP generates excellent visualization for every data set in general, with the majority of the clusters well separated. However, it fails to separate some clusters that are very similar to each other and fails to reveal the subtle subclusters as we see for the Fashion-MNIST and MNIST data sets with various min_dist values. It is not sufficient to get a finer cluster structure by reducing only the value of min_dist . Manually decreasing the values of the parameters α^* and b^* in UMAP might be needed.

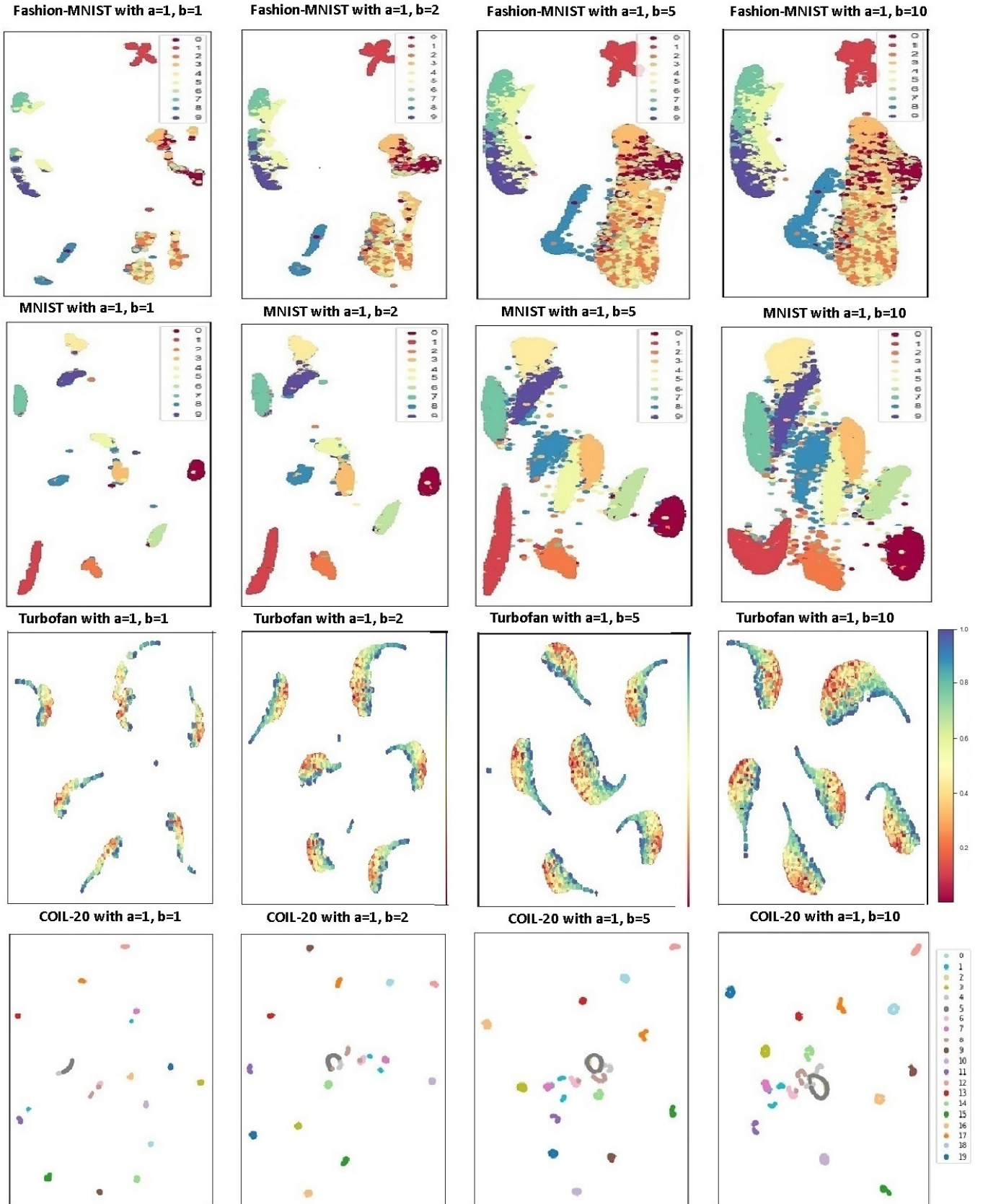


Figure 3: Visualizations of real-world data sets with $b = 1, 2, 5,$ and $10,$ respectively.

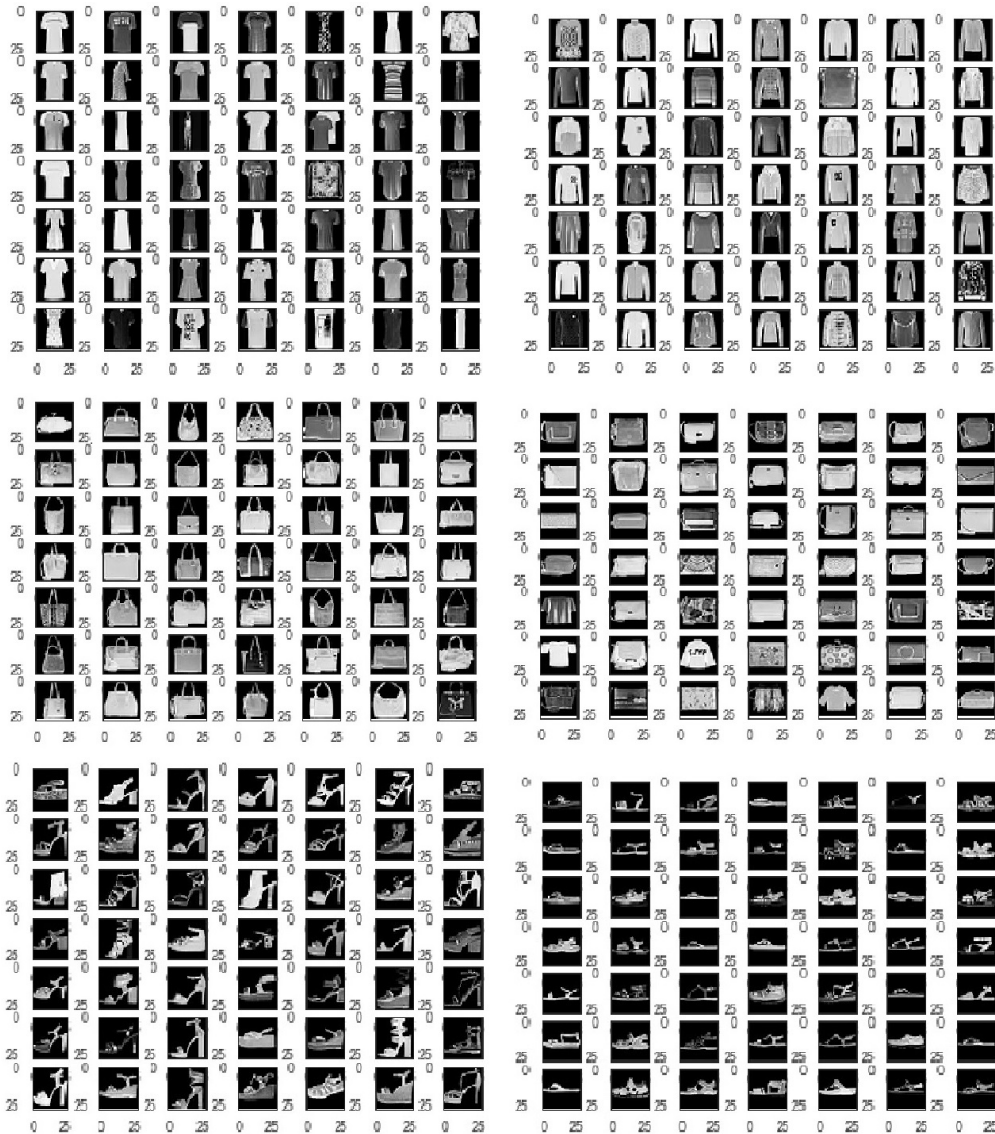


Figure 4: Image comparisons for Fashion-MNIST data. The first row shows the cluster of T-shirts and dresses versus the cluster of coats, pullovers, and shirts. The second row shows the subclusters of bags with and without handles. The third row shows the subclusters of sandals with and without heels.

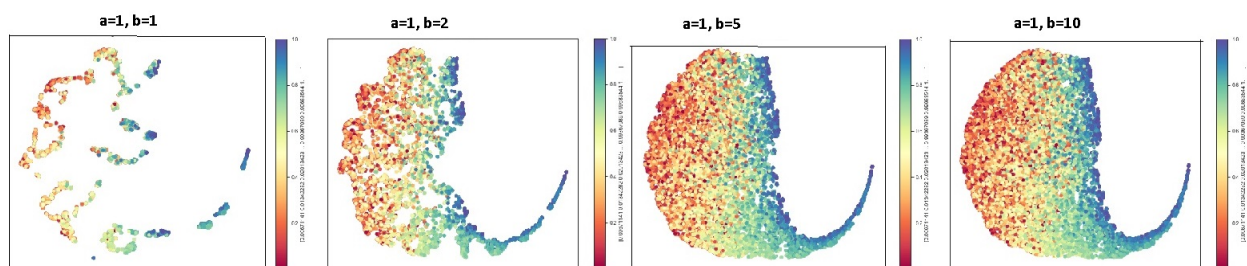


Figure 5: Visualization of Turbofan Engine Degradation Simulation data after removing the impact of different flight conditions.

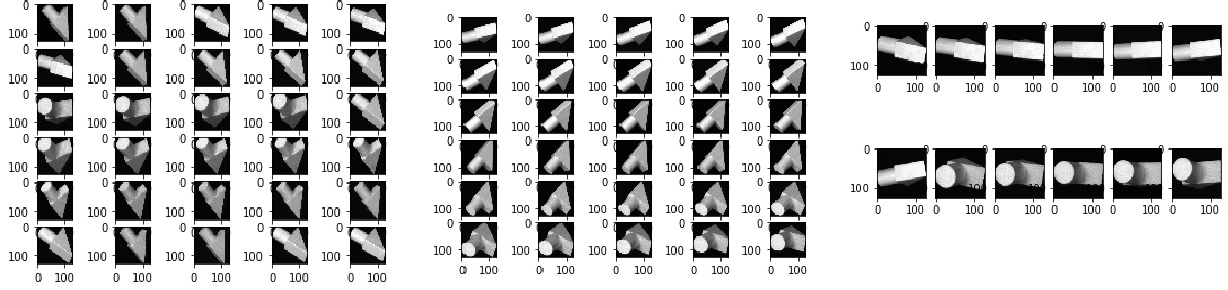


Figure 6: Images for object 1 from three subclusters. The arrows from subcluster 1 mainly point downward. The arrows from subcluster 2 mainly point upward. The arrows from subcluster 3 mainly point horizontally.

4 Conclusions

In this paper, we propose using a generalized sigmoid function to model the distance similarity in both high-dimensional and low-dimensional spaces. In particular, the parameter b is introduced to the generalized sigmoid function in low-dimensional space. By changing the value of b , we can adjust the heaviness of the function tail. Using both simulated and real data sets, we show that decreasing the value of b can help us reveal the finer cluster structure of the data. Using visualization and domain knowledge, we show that the subclusters in the Fashion-MNIST, MNIST, Turbofan Engine Degradation Simulation, and COIL-20 data sets are meaningful.

In practice, however, as with the finding in UMAP that a low value of min_dist might lead you to spuriously interpret the data structure, a small value of b might also result in the discovery of some clusters of random sampling noise. In addition, we learn from the curves with varying b values that the smaller the value b is, the flatter the tail of the curve is. So embedding convergence might be slower with a low value of b , especially when the sample size is small, the number of features is high, and there are many clusters. For example, the COIL-20 data set has only 1,440 images of 20 different objects, but the images have 16,384 features. In order to get a stable embedding, we increase the number of epochs to 5,000 with small b values.

In the literature of information visualization, how to assess the quality of graph visualizations is a long-standing problem. If the purpose of the study is classification or data exploration, then reducing the value of b properly might give us more insights into the data structure. However, if the purpose of the study is to maintain pairwise distance of neighbors in high-dimensional space, then reducing the value of b can also reduce the continuity of the neighbors. In practice, there is no unanimous criterion for choosing the b value. We suggest trying out different b values for data exploration to get a comprehensive understanding of the data.

5 Acknowledgments

The authors would like to thank Ed Huddleston, Senior Technical Editor for his assistance in editing this paper, and Anya McGuirk, Distinguished Research Statistician Developer, and Byron Biggs, Principal Research Statistician Developer, for their advice and comments.

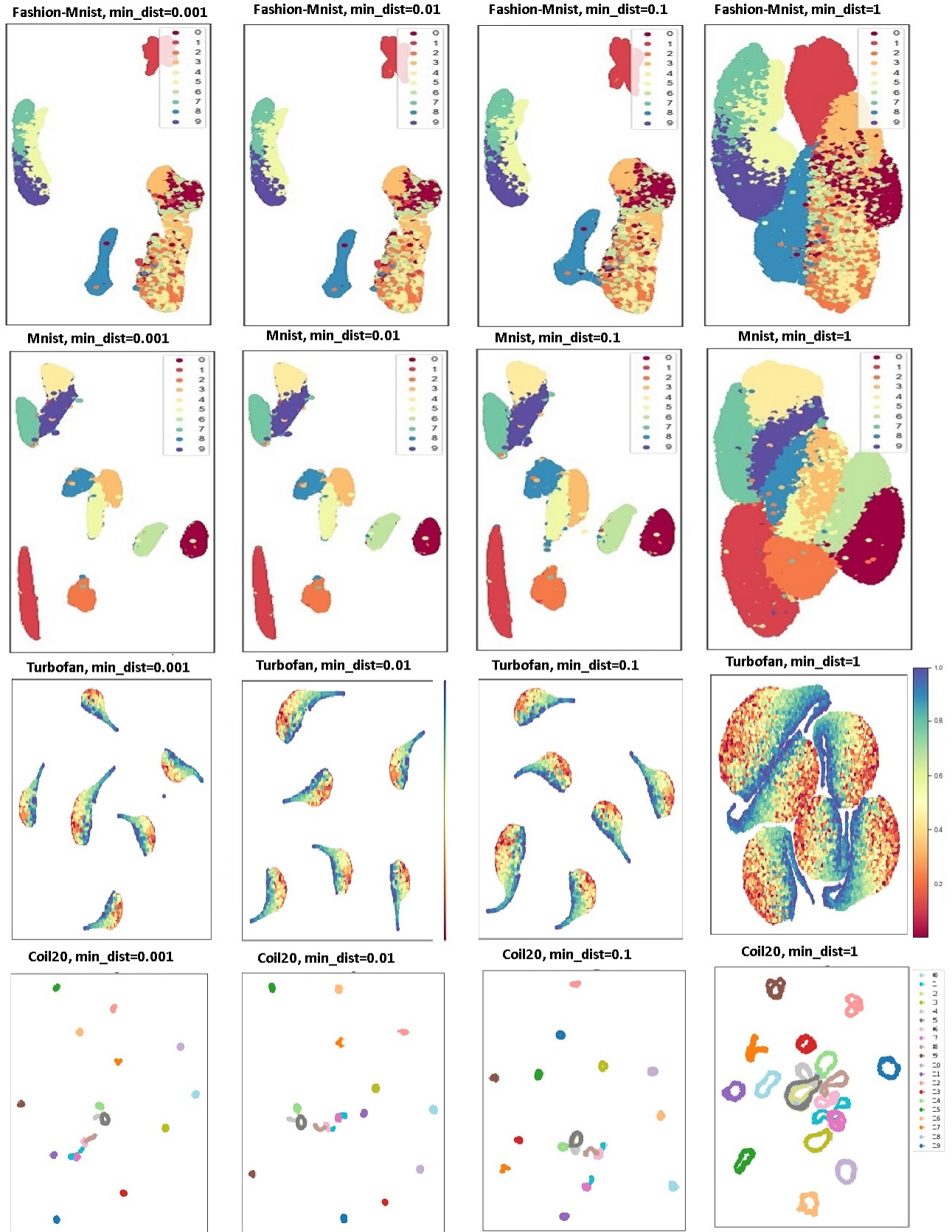


Figure 7: Visualizations of real-world data sets by UMAP by setting $min_dist = 0.001, 0.01, 0.1,$ and 1 .

References

- [1] Belkin, M., and Niyogi, P. (2002). “Laplacian Eigenmaps and Spectral Techniques for Embedding and Clustering.” In *Advances in Neural Information Processing Systems*, 585–591. Cambridge, MA: MIT Press.
- [2] Borg, I., and Groenen, P. J. (2005). *Modern Multidimensional Scaling: Theory and Applications*. New York: Springer Science and Business Media.
- [3] Ceriotti, M., Tribello, G. A., and Parrinello, M. (2011). “Simplifying the Representation of Complex Free Energy Landscapes Using Sketch-Map.” *Proceedings of the National Academy of Sciences* 108:13023–13028.
- [4] Cook, J., Sutskever, I., Mnih, A., and Hinton, G. (2007). “Visualizing Similarity Data with a Mixture of Maps.” In *Artificial Intelligence and Statistics*, 67–74. San Juan, Puerto Rico.
- [5] Demartines, P., and Hérault, J. (1997). “Curvilinear Component Analysis: A Self-Organizing Neural Network for Nonlinear Mapping of Data Sets.” *IEEE Transactions on Neural Networks* 8:148–154.
- [6] Hinton, G. E., and Roweis, S. T. (2003). “Stochastic Neighbor Embedding.” In *Advances in Neural Information Processing Systems*, 857–864. Cambridge, MA: MIT Press.
- [7] Hotelling, H. (1933). “Analysis of a Complex of Statistical Variables into Principal Components.” *Journal of Educational Psychology* 24:417.
- [8] Kobak, D., Linderman, G., Steinerberger, S., Kluger, Y., and Berens, P. (2019). “Heavy-Tailed Kernels Reveal a Finer Cluster Structure in t-SNE Visualisations.” arXiv preprint, arXiv:1902.05804.
- [9] Lecun, Y., and Cortes, C. (2012). “The MNIST Database of Handwritten Digit Images for Machine Learning Research.” *IEEE Signal Processing Magazine* 29:141–142.
- [10] McInnes, L., Healy, J., and Melville, L. (2018). “UMAP: Uniform Manifold Approximation and Projection for Dimension Reduction.” arXiv preprint, arXiv:1802.03426.
- [11] Mikolov, T., Sutskever, I., Chen, K., Corrado, G. S., and Dean, J. (2013). “Distributed Representations of Words and Phrases and Their Compositionality.” In *Advances in Neural Information Processing Systems*, 3111–3119. La Jolla, CA: Neural Information Processing Systems Foundation.
- [12] Nene, S. A., Nayar, S. K., Murase, H., et al. (1996). Columbia Object Image Library (COIL-20).
- [13] Saxena, A., and Goebel, K. (2008). Turbofan Engine Degradation Simulation data set. NASA Ames Prognostics Data Repository, NASA Ames Research Center, Moffett Field, CA.
- [14] Tang, J., Liu, J., Zhang, M., and Mei, Q. (2016). “Visualizing Large-Scale and High-Dimensional Data.” In *Proceedings of the 25th International Conference on World Wide Web*, 287–297. Geneva: International World Wide Web Conferences Steering Committee.
- [15] Tang, J., Qu, M., Wang, M., Zhang, M., Yan, J., and Mei, Q. (2015). “LINE: Large-Scale Information Network Embedding.” In *Proceedings of the 24th International Conference on World Wide Web*, 1067–1077. Geneva: International World Wide Web Conferences Steering Committee.
- [16] Tenenbaum, J. B., De Silva, V., and Langford, J. C. (2000). “A Global Geometric Framework for Nonlinear Dimensionality Reduction.” *Science* 290:2319–2323.
- [17] Torgerson, W. (1952). “The First Major MDS Breakthrough.” *Psychometrika* 17:401–419.

- [18] Van der Maaten, L. (2014). “Accelerating t-SNE Using Tree-Based Algorithms.” *Journal of Machine Learning Research* 15:3221–3245.
- [19] Van der Maaten, L., and Hinton, G. (2008). “Visualizing Data Using t-SNE.” *Journal of Machine Learning Research* 9:2579–2605.
- [20] Xiao, H., Rasul, K., and Vollgraf, R. (2017). “Fashion-MNIST: A Novel Image Dataset for Benchmarking Machine Learning Algorithms.” arXiv preprint, arXiv:1708.07747.